ACS APPLIED MATERIALS & INTERFACES

Research Article

www.acsami.org

Role of Vertical Segregation in Semitransparent Organic Photovoltaics

Alexander Kovalenko,[†,‡] Antonio Guerrero,*[,†] and Germà Garcia-Belmonte*[,†]

[†]Photovoltaic and Optoelectronic Devices Group, Departament de Física, Universitat Jaume I, ES-12071 Castelló, Spain

[‡]Brno University of Technology, Faculty of Chemistry, Materials Research Centre, Purkyňova 118, 612 00 Brno, Czech Republic

Supporting Information

ABSTRACT: In this work, the efficiency of semitransparent organic photovoltaic (OPV) devices for low intensity applications is investigated as a function of the processing conditions. It is observed that a thermal treatment of the organic layer induces fullerene migration toward the active layer/air interface. This physical process gives rise to different vertical segregation profiles of donor and acceptor molecules. Once the back contact is deposited, the amount of fullerene covering the surface will determine the contact selectivity and leakage current of the device. Control of this leakage current may not be essential for devices fabricated for high illumination condition applications. However, devices to be used under low illumination conditions may be highly influenced by the presence of this parasitic dark current which flows in the opposite direction to photogenerated current. At the proximity of the contacts, the vertical segregation profile is inferred from optical and electrical measurements. In particular, external quantum efficiency (EQE) measurements carried out from a relatively opaque back contact provide local information on the materials spatially close to the light source. Alternatively, capacitance–voltage measurements enable calculation of the percentage of fullerene molecules covering the cathode contact. Overall, a versatile method that can be used in regular and inverted configuration is presented that explains the different behavior observed for devices to be used under low illumination conditions.

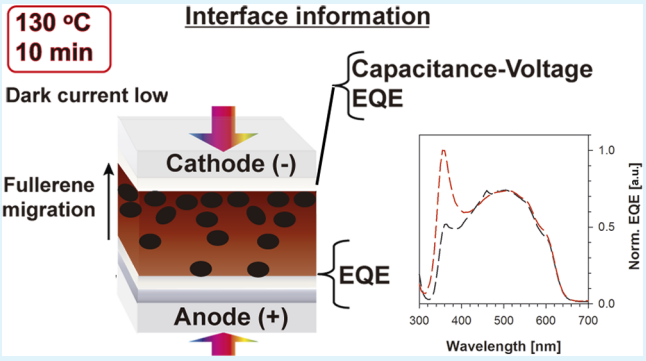

KEYWORDS: *organic photovoltaics, low illumination conditions, contact selectivity, capacitance–voltage, impedance spectroscopy*

INTRODUCTION

Organic photovoltaics (OPV) have been studied for nearly 30 years, and the technology is now on the verge of commercialization. With record power conversion efficiencies slightly exceeding 10%, OPV still lag behind other technologies such as silicon-based photovoltaics that can provide 20% in modules.[1] However, the benefits of OPV rely on the possibility to produce flexible and low weight products with a high degree of design freedom with very rapid payback times.[2] In addition, it has been claimed that OPV can outperform silicon technology under low light conditions.[3] These advantages and the ease of handling in subsequent product-integration processes will enable its implementation into new consumer and portable electronics such as building-integrated photovoltaic (BIPV) products. "Futuristic" products with value-added applications may be envisaged such as the use of semitransparent windows BIPV that permit both natural or color designed room illumination with production of solar electricity. Such a semitransparent device could additionally function during the night as a room light scavenger working under low illumination conditions to recover part of the "wasted" illumination energy.

The search for new semitransparent electrodes has made available a range of materials such as thin Ag electrodes, Ag nanowires,[4] free-standing carbon nanotubes,[5] or highly conductive PEDOT:PSS.[6] Using all the knowledge learned from OPVs during the past decade, semitransparent devices with conversion efficiencies (PCE) as high as 5.4% in a single layer[7] or 7% in tandem configuration[8] have been obtained with average transmission of 30%. Alternatively, PCE of 6.4% have been achieved with a maximum transmission of 51% at 550 nm in the tandem configuration.[8] Unfortunately, any information related to the physical requirements or working principles for devices to be used under low light intensities is rather scarce.

It is well-known that morphology of the donor/acceptor blend of the organic layer is a critical aspect toward the final device efficiency.[9,10] For this reason, several processing conditions have been developed which enable adequate morphology in the bulk of the organic blend.[11] Additionally, selectivity of the contacts play a very important role, as an adequate vertical phase segregation of the donor and acceptor

Received: October 20, 2014
Accepted: December 19, 2014
Published: December 19, 2014

DOI: 10.1021/am5071859
ACS Appl. Mater. Interfaces 2015, 7, 1234–1239

molecules is required where the fullerene molecules are in close contact with the selective layer to electrons and the polymer with the electrode selective to holes.[12,13] For example, it is known that a thermal or solvent annealing is an essential procedure for standard P3HT:PCBM bulk heterojunction (BHJ) solar cells to improve solar cells efficiency by creating appropriate morphology and vertical phase segregation.[14] Importantly, this vertical segregation depends on the substrate where the organic layer is deposited and different device architectures may be designed to enable contacts rich on either polymer or fullerene.[12]

A range of different techniques has been developed to study segregation of donor and acceptor molecules within the active layer.[15] Among the different types, some provide 3D structural information on the bulk of the active layer and include grazing incidence X-ray diffraction (GIXRD), variable-angle spectroscopic ellipsometry (VASE), transmission electron microscopy (TEM), or secondary ion mass spectrometry (SIMS).[16] Alternatively, other techniques look into the active layer/air interface and include techniques such as atomic force microscopy (AFM), scanning electron microscopy (SEM), or capacitance−voltage (C−V). The above-mentioned techniques are complementary, and each presents their own limitations that make them inaccessible to many research laboratories. For example, most of them require sophisticated and expensive equipment (GIXRD or TEM); some are destructive (SIMS, GIXRD or TEM), and most do not allow the measurement on working devices with the exception of C−V and VASE (if very thin contact layers are used). As a drawback, they are both nondirect techniques that require mathematical estimations. Of particular interest for the purpose of the present work is the use of a purely electrical technique such as C−V, able to provide information on the donor/acceptor ratio at the cathode contact in completed devices.[13]

This work is focused on providing a clear understanding about the role of contact selectivity on semitransparent devices operating under low illumination conditions. For the different configurations studied, a thermal treatment induces the migration of fullerene molecules toward the active layer/air interface which will ultimately determine the contact selectivity. Shunt resistance under varied illumination (photoshunt) is observed to be a determining parameter especially under low irradiation. Indeed, the selection of regular or inverted architecture as well as the processing conditions is a critical feature to take into account for devices to be used under low illumination conditions.

EXPERIMENTAL SECTION

Materials. P3HT (Luminescence Technology Corp.), PCBM ($PC_{60}BM$, Solenne, 99%), *o*-dichlorobenzene (Aldrich, 99.9%), PEDOT:PSS (CLEVIOS P Al 4083), ZnO (Gene's Ink, SC041-DIG), Ca (Aldrich, 99.995%), MoO_3 (Aldrich, 99.98%), and Ag (Aldrich, 99.99%) were used as received without further purification. Prepatterned ITO (Xin Yan, XY10S) was cleaned with detergent and sonication followed by several rinsing steps with water, ethanol, and isopropanol. Organic matter was removed by introducing the substrates into an UV−ozone chamber for 15 min. The active layer films were prepared from the P3HT:PCBM solution (1:0.8 by weight) in *o*-dichlorobenzene (17 mg mL^{-1}) and were stirred at 80 °C for 12 h until complete dissolution. The concentration in *o*-dichlorobenzene solvent of the pure P3HT and PCBM solutions were 17 and 13.6 mg mL^{-1}, respectively. All manipulations were carried out in a glovebox under a nitrogen atmosphere unless otherwise stated.

Device Fabrication. For the regular device architecture, glass substrates with patterned ITO were covered by PEDOT:PSS by spin coating at 5500 rpm for 60 s. Films were dried by annealing for 10 min at 120 °C in air followed by a further thermal treatment in the glovebox for another 10 min at 110 °C to remove residual moisture. In the case of inverted architecture, ZnO nanoparticles dispersed in isopropanol were deposited by the spin-coating procedure at 1000 rpm for 40 s onto the glass/ITO substrates to form a 30 nm layer and then annealed for 30 s at 75 °C. The polymer−fullerene heterojunction layer was created by spin coating 55 μL of prepared P3HT:PCBM solution at 1200 rpm for 15 s; the wet film was solvent annealed in a Petri dish for 60 min. Half of the considered devices was further thermally treated at 130 °C for 10 min to obtain the second set of processing conditions (solvent + thermal annealed). Top electrodes were deposited by sequential evaporation of Ca (7) and Ag (30 nm). Alternatively, for inverted devices, MoO_3 (5 nm)/Ag(25 nm) was evaporated. In both type of device configurations, semitransparent back electrodes were obtained. A total of 10 devices were measured using each of the conditions mentioned above.

Characterization Techniques. Film thickness was determined by a VEECO DEKTACK 6 M Stylus Profiler. The current density−voltage measurements were carried out under illumination using an Abet Sun 2000 solar simulator with an air mass (AM) 1.5G filter. The simulated light intensity was adjusted to 1000 W m^{-2} by using a NREL-calibrated Si solar cell. Low illumination conditions were created by using calibrated perforated sheets commercially available (ABET) which do not modify the spectrum of the light while maintaining the light homogeneity. External quantum efficiency (EQE) measurements were performed using a 150 W Xe lamp coupled with a monochromator controlled by a computer. The light intensity was measured using an optical power meter 70310 from Oriel Instruments where a Si photodiode was used to calibrate the system. Capacitance−voltage data were measured using an Autolab PGSTAT-30 equipped with a frequency analyzer module; small voltage perturbation (20 mV rms) at 1000 Hz was applied in dark conditions.

RESULTS AND DISCUSSION

A set of semitransparent devices was prepared in the configuration ITO/PEDOT:PSS/P3HT:PCBM/Ca/Ag as displayed in Figure 1. Semitransparency of the back electrode provided maximum transmittance of 26% at 440 nm and average transparency in the visible region (390−700 nm) of

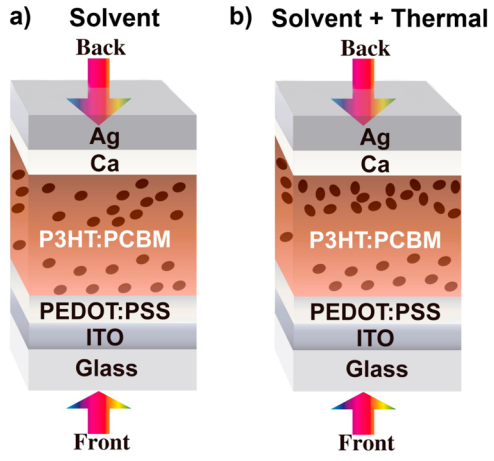

Figure 1. Scheme of the semitransparent device configuration indicating the different processing conditions used. Devices have been illuminated either from the ITO/PEDOT:PSS (front) or from the semitransparent Ca/Ag electrode (back). Fullerenes migration induced by thermal treatment is schematically represented by showing a higher concentration of dots (fullerenes) close to the Ca/Ag electrode.

DOI: 10.1021/am5071859
ACS Appl. Mater. Interfaces 2015, 7, 1234−1239

Table 1. Parameters of the Polymer–Fullerene Devices

	illumination from ITO/PEDOT:PSS					illumination from Ag/Ca					capacitance voltage		J–V dark conditions
	J_{SC} [mAcm^{-2}]	V_{OC} [mV]	FF [%]	η [%]	R_{sh}, [Ωcm^{-2}]	J_{SC} [mAcm^{-2}]	V_{OC} [mV]	FF [%]	η [%]	R_{sh}, [Ωcm^{-2}]	[V], V	fullerene cathode coverage [%]	leakage current at −1 V [mAcm^{-2}]
solvent	7.49	614	59	2.71	1269	2.21	570	62	0.78	4404	0.43	68	0.57
solvent + thermal	7.01	617	60	2.59	2036	1.80	574	62	0.64	6482	0.35	97	0.18

15% that allows illumination from both sides (see Supporting Information Figure SI1). Two different approaches to provide adequate morphology were followed: in the first, the organic layer was spin coated and when still wet was introduced into a Petri dish to slowly dry the organic layer during 1 h. In a second method, after solvent annealing devices were thermally treated at 120 °C for 10 min. These two set of conditions will be denoted in the manuscript as solvent annealing and solvent + thermal annealing, respectively. The bulk morphology of the films using the different conditions did not differ significantly in terms of domain size/shape as can be observed in the dark field TEM images shown in the Supporting Information (Figure SI2). Devices were electrically and optically characterized by using different techniques.

Device performance parameters were analyzed under different light intensity conditions using a solar simulator. Here, the spectrum of 1.5G (AM) was not modified by using metal perforated sheets to reduce the power intensity while maintaining the light homogeneity. Efficiency of photovoltaic devices is calculated as a function of the light intensity of the illumination source as PCE = $(J_{sc} \times V_{oc} \times FF)/I_0$, where J_{sc} is the current density at short circuit, V_{oc} is the open circuit voltage, FF is the fill factor, and I_0 is the light intensity of the source. Both processing conditions provided similar PCE under one sun light intensity condition as shown in Table 1 (front illuminated ~2.6–2.7%). Interestingly, when the light intensity is reduced, only the device processed using both solvent and thermal annealing retains the efficiency under low light intensity conditions. On the other hand, the device solvent annealed dramatically reduces the PCE, and at 330 Wm^{-2}, the efficiency is already half of that observed at 1 sun (Figure 2). Interestingly, this drop in efficiency clearly correlates with a drop in the achievable photocurrent of the device. Here, the J_{sc} has been normalized to take into account the difference in light intensity. In order to provide an understanding for these observations, further electrical measurements were carried out.

Current density vs voltage curves of devices was measured from both semitransparent sides being front and back illuminated as depicted in Figure 1, ITO/PEDOT:PSS (front) and Ca/Ag (back). In both measurements, devices processed with only solvent annealing provided slightly better performance as shown in Figure 3 in good agreement with previously reported data for P3HT:PCBM with similar levels of transparency.[14] Efficiency parameters are in the range of 2.7% illuminating from the front and drops to about 0.7% if illuminated from the Ca/Ag side as a significant part of the light is absorbed/reflected by the metal layers. Interestingly, if we take into account the low transparency of the back contact, efficiency when the device is illuminated from Ca/Ag is remarkably high. Fill factors are in the order of 60% and slightly increased when illuminated from the back electrode. The obtained high efficiency when illuminated from the Ca/Ag electrode correlates with an improvement in the fill factor and an increase of the shunt resistance.

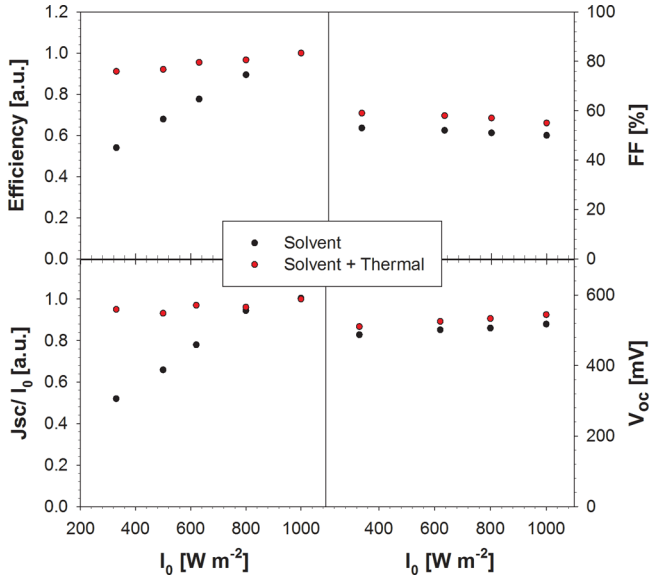

Figure 2. Performance parameters measured under different light intensity conditions. While PCE of devices processed using solvent annealing conditions are dramatically reduced, mainly due to a decrease in photocurrent, devices which undertook a further thermal annealing maintain the efficiency.

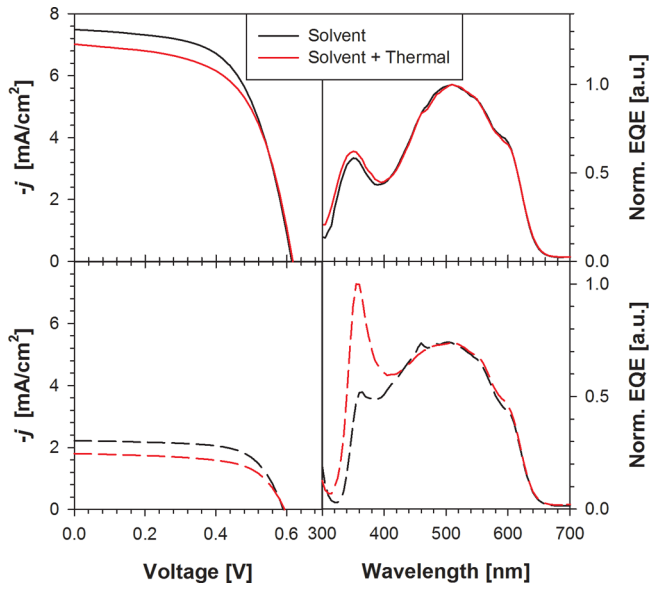

Figure 3. J–V curves of P3HT:PCBM devices processed either by solvent annealing or by having an additional thermal treatment. Normalized external quantum efficiency of measurements carried out from the devices that have been either illuminated from the ITO or from the semitransparent silver electrode (back).

External quantum efficiency (EQE) measurements are shown in Figure 3. When devices are illuminated from the front

DOI: 10.1021/am5071859
ACS Appl. Mater. Interfaces 2015, 7, 1234–1239

contact (ITO/PEDOT:PSS), no noticeable spectra differences are observed between the two processing conditions. Strikingly, when EQE is recorded by illumination from the back electrode, the relative contribution to the photocurrent of PCBM (<450 nm) and P3HT (~400−650 nm) is seriously affected by the processing conditions used in each device. Therefore, EQE measurement illuminating from the back electrode (highly opaque) provides local information on the materials actually close to the semitransparent contact. It is important to note that EQE is in general a technique carried out under low illumination conditions and its use by illumination of the back contact further reduces the intensity of the light. Therefore, the local concentration may be detected as a result of using both low light intensity and materials with a high extinction coefficient in the organic layer. This correlation of EQE response and local information on the back contact will be further supported below for devices prepared with an inverted configuration. For the regular configuration, the relative fullerene/polymer intensity ratio of EQE peaks increases for the device thermally annealed, thus indicating that fullerene molecules contribute more to the photocurrent than in the case of solvent annealed devices. These results can be explained in terms of vertical segregation of the fullerene polymer across the active layer. This would be the result of PCBM molecules migrating toward the active layer/air interface by the use of the thermal treatment. Therefore, once the cathode contact is deposited, fullerene molecules will be in contact with the Ca/Ag improving the contact selectivity as it will be discussed below.[12]

We have previously described a method to calculate the proportion of fullerene molecules in close contact with the cathode which relies on a purely electrical technique such as capacitance−voltage.[13] In this methodology, the flat-band potential (V_{FB}) or potential required to provide a flat band profile is correlated with the band-bending of the organic layer at the vicinity of the cathode and generation of a dipole at the interface.[17] The magnitude of such a dipole depends on the amount of fullerene molecules in contact with the cathode being higher for a high proportion of fullerene molecules which in turns reduces the magnitude of the V_{FB}. This method has already been used for a range of materials such as PTB7:$PC_{71}BM$.[18,19] In addition, fullerene content calculated with this method correlates with other advanced microscopy techniques such as the nanoscale mapping by electron energy-loss spectroscopy.[20] It is important to note that the final proportion of fullerene/polymer at the top of the active layer blend is highly dependent not only on the processing conditions of the active layer but also on the substrate on which the active layer is deposited.[12] Indeed, formation of a skin layer of polymer has also been observed in the literature.[21−23] Here, we observe that V_{FB} shifts significantly with the processing conditions from 0.47 V (solvent) to 0.35 V (solvent + thermal). Preparing devices with full coverage of either polymer or fullerene (see Supporting Information), we can correlate these V_{FB} values with fullerene coverage of 97% and 68%, respectively. Therefore, on the basis of these results, it can be clearly concluded that devices processed using solvent and thermal annealing show high cathode coverage by fullerene molecules. Therefore, high electron selectivity of the cathode contact is assured by the presence of fullerene molecules contacting the cathode.

The current measured under dark conditions that can be extracted from the diode curves at negative bias is known to be a measurement of the leakage current of the device (Figure 4a); results are summarized in Table 1. Values of the leakage current

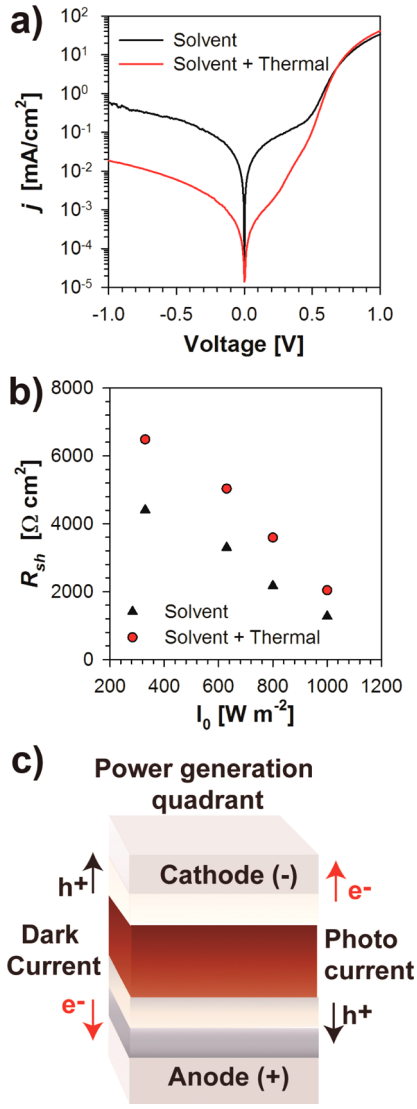

Figure 4. (a) Diode curve measured under dark conditions for the two devices under study. (b) Variation of shunt resistance as a function of the light intensity. (c) Scheme of current flow for dark current and photocurrent in the power generation quadrant.

are proposed as a guide on the selectivity of the contacts encountered at high illumination conditions. High current at negative bias and low shunt resistance is then a clear sign of devices with contacts poorly selective. Figure 4b shows how R_{sh} increases with a reduction of the light intensity for both devices. However, the difference between values is small at 1 sun light intensity (930 Ω cm^2) increasing at low illumination conditions (2054 Ω cm^2). Similarly, when the device is illuminated from Ca/Ag, the light intensity is reduced and R_{sh} increases to similar levels as those observed for illumination from the ITO side at low light intensity levels; see Table 1. This behavior relates to the occurrence of a light-dependent leakage current giving rise to a photoshunt[24] presumably related to the selectivity features of the cathode contact. Importantly, at low illumination conditions, there is a clear competition between the dark and photogenerated currents as both flow in opposite directions as depicted in Figure 4c. Indeed, the dark current at negative bias

DOI: 10.1021/am5071859
ACS Appl. Mater. Interfaces 2015, 7, 1234−1239

(−1 V) for the device only solvent annealed (0.57 mA cm^{-2}) represents already 50% of the obtained J_{sc} at 330 Wm^{-2} (1.13 mA cm^{-2}). For comparison purposes, the J_{sc} obtained at the different light intensity conditions for the solvent annealed devices is shown in Figure 2. In this case, the observed photocurrent decrease at low illumination conditions is clearly connected with the relative increase in leakage current and the low proportion of fullerene molecules covering the cathode contact. Importantly, no difference in the expected photocurrent is observed for a device that shows a highly selective cathode as that obtained from the solvent and thermal annealing. This correlation between fullerene coverage at the cathode, contact selectivity, and leakage current suggests an interfacial origin for the photoshunt effect shown in Figure 4b, although our measurements are not conclusive and do not allow one to discard a bulk origin for the light-dependent leakage current.

Interestingly, in an inverted configuration (ITO/ZnO/P3HT:PCBM/MoO_3/Ag), there is a similar behavior to that observed in the regular configuration where the contact selectivity may be modified by the processing conditions of the active layer. It is important to note that in the regular configuration EQE and C−V provide information on the same contact (Ca/Ag). Alternatively, in the inverted configuration, EQE provides information on the anode (MoO_3/Ag) and C−V on the cathode (ZnO/ITO). The same set of processing conditions has been tested for the inverted configuration, but for simplicity, we do not discuss here the details; full information is shown as Supporting Information. Again, in the inverted configuration, the thermal treatment promotes the transport of fullerene molecules toward the active layer/air interface where the contact selective to holes will be deposited (MoO_3/Ag). This high coverage of fullerene molecules of the anode contact is detected by the EQE measurements where the relative contribution of fullerene will be enlarged as compared to the devices prepared with only a solvent annealing treatment. This large fullerene coverage is in good agreement with the expected high leakage current at negative bias as the fullerenes have migrated to the selective collector to the opposite electrode. Overall, in the two systems under study, the thermal treatment promotes the migration of fullerene molecules to the active layer/air interface. While in the regular configuration, this will improve the contact selectivity as fullerenes are close to the selective layer to electrons; in the inverted configuration, the effect will be the opposite.

CONCLUSIONS

In the present work, the high impact of vertical segregation of donor and acceptor molecules on the contact selectivity of devices to be used for low intensity applications is explored. It is observed that a thermal treatment of the organic layer induces the fullerene migration toward the active layer/air interface. The amount of fullerene molecules covering the surface will determine the contact selectivity and leakage current of the device once the back contact is deposited. Control of this leakage current may not be essential for devices fabricated for high illumination condition applications. However, devices to be used under low illumination conditions may be highly influenced by the presence of this parasitic dark current which flows in the opposite direction to photogenerated current. The present work provides some tools to better understand the difference in the limitations observed for devices to be used under low illumination conditions. By using a combination of optical and electrical techniques, we are able to show that devices which contain a high proportion of fullerene molecules at the cathode are highly selective and do not suffer from shunting. The extracted conclusions not only are applicable to organic photovoltaic devices but also can be extrapolated to photodetectors where the leakage needs to be minimized (the dark current should be minimized in order to enhance the sensitivity/responsitivy of the detector).

ASSOCIATED CONTENT

Supporting Information

Data on contacts and device transparency, film morphology, information to calculate fullerene content by C−V, and an analogous study for inverted device configuration. This material is available free of charge via the Internet at http://pubs.acs.org/.

AUTHOR INFORMATION

Corresponding Authors

*E-mail: aguerrer@uji.es.
*E-mail: garciag@uji.es.

Notes

The authors declare no competing financial interest.

ACKNOWLEDGMENTS

This work was partially supported by FP7 European collaborative project SUNFLOWER (FP7-ICT-2011-7-contract num. 287594) and Generalitat Valenciana (project ISIC/2012/008 Institute of Nanotechnologies for Clean Energies). A.K. acknowledges Brno University of Technology for financial support (CZ.1.07/2.3.00/30.0039). We thank Prof. Sara Bals and Dr. Martin Pfannmöller from EMAT (University of Antwerp) for kindly providing dark field TEM images of films.

REFERENCES

(1) Green, M. A.; Emery, K.; Hishikawa, Y.; Warta, W.; Dunlop, E. D. Solar Cell Efficiency Tables (version 39). *Prog. Photovoltaics* **2012**, *20*, 12−20.

(2) Darling, S. B.; You, F. The Case for Organic Photovoltaics. *RSC Adv.* **2013**, *3*, 17633−17648.

(3) Roland Steim, T. A.; Schilinsky, P.; Waldauf, C.; Dennler, G.; Scharber, M.; Brabec, C. J. Organic Photovoltaics for Low Light Applications. *Sol. Energy Mater. Sol. Cells* **2011**, *95*, 3256−3261.

(4) Reinhard, M.; Eckstein, R.; Slobodskyy, A.; Lemmer, U.; Colsmann, A. Solution-Processed Polymer−Silver Nanowire Top Electrodes for Inverted Semi-Transparent Solar Cells. *Org. Electron.* **2013**, *14*, 273−277.

(5) Kim, Y. H.; Sachse, C.; Zakhidov, A. A.; Meiss, J.; Zakhidov, A. A.; Müller-Meskamp, L.; Leo, K. Combined Alternative Electrodes for Semi-Transparent and ITO-Free Small Molecule Organic Solar Cells. *Org. Electron.* **2012**, *13*, 2422−2428.

(6) Zhou, Y.; Cheun, H.; Choi, S.; Potscavage, W. J.; Fuentes-Hernandez, C.; Kippelen, B. Indium Tin Oxide-Free and Metal-Free Semitransparent Organic Solar Cells. *Appl. Phys. Lett.* **2010**, *97*, 153304.

(7) Betancur, R.; Romero-Gomez, P.; Martinez-Otero, A.; Elias, X.; Maymo, M.; Martorell, J. Transparent Polymer Solar Cells Employing a Layered Light-trapping Architecture. *Nat. Photonics* **2013**, *7*, 995−1000.

(8) Chen, C.-C.; Dou, L.; Gao, J.; Chang, W.-H.; Li, G.; Yang, Y. High-Performance Semi-Transparent Polymer Solar Cells Possessing Tandem Structures. *Energy Environ. Sci.* **2013**, *6*, 2714−2720.

(9) Yang, X.; Loos, J. Toward High-Performance Polymer Solar Cells: The Importance of Morphology Control. *Macromolecules* **2007**, *40*, 1353−1362.

DOI: 10.1021/am5071859
ACS Appl. Mater. Interfaces 2015, 7, 1234−1239

(10) Yang, X.; Loos, J.; Veenstra, S. C.; Verhees, W. J. H.; Wienk, M. M.; Kroon, J. M.; Michels, M. A. J.; Janssen, R. A. J. Nanoscale Morphology of High-Performance Polymer Solar Cells. *Nano Lett.* **2005**, *5*, 579−583.
(11) Li, G.; Zhu, R.; Yang, Y. Polymer Solar Cells. *Nat. Photonics* **2012**, *6*, 153−161.
(12) Campoy-Quiles, M.; Ferenczi, T.; Agostinelli, T.; Etchegoin, P. G.; Kim, Y.; Anthopoulos, T. D.; Stavrinou, P. N.; Bradley, D. D. C.; Nelson, J. Morphology Evolution via Self-Organization and Lateral and Vertical Diffusion in Polymer:Fullerene Solar Cell Blends. *Nat. Mater.* **2008**, *7*, 158−164.
(13) Guerrero, A.; Dörling, B.; Ripolles-Sanchis, T.; Aghamohammadi, M.; Barrena, E.; Campoy-Quiles, M.; Garcia-Belmonte, G. Interplay Between Fullerene Surface Coverage and Contact Selectivity of Cathode Interfaces in Organic Solar Cells. *ACS Nano* **2013**, *7*, 4637−4646.
(14) Li, G.; Shrotriya, V.; Huang, J.; Yao, Y.; Moriarty, T.; Emery, K.; Yang, Y. High-Efficiency Solution Processable Polymer Photovoltaic Cells by Self-Organization of Polymer Blends. *Nat. Mater.* **2005**, *4*, 864−868.
(15) Chen, W.; Nikiforov, M. P.; Darling, S. B. Morphology Characterization in Organic and Hybrid Solar Cells. *Energy Environ. Sci.* **2012**, *5*, 8045−8074.
(16) Liu, F.; Gu, Y.; Shen, X.; Ferdous, S.; Wang, H.-W.; Russell, T. P. Characterization of the Morphology of Solution-Processed Bulk Heterojunction Organic Photovoltaics. *Prog. Polym. Sci.* **2013**, *38*, 1990−2052.
(17) Guerrero, A.; Marchesi, L. F.; Boix, P. P.; Ruiz-Raga, S.; Ripolles-Sanchis, T.; Garcia-Belmonte, G.; Bisquert, J. How the Charge-Neutrality Level of Interface States Controls Energy Level Alignment in Cathode Contacts of Organic Bulk-Heterojunction Solar Cells. *ACS Nano* **2012**, *6*, 3453−3460.
(18) Guerrero, A.; Montcada, N. F.; Ajuria, J.; Etxebarria, I.; Pacios, R.; Garcia-Belmonte, G.; Palomares, E. Charge Carrier Transport and Contact Selectivity Limit the Operation of PTB7-Based Organic Solar Cells of Varying Active Layer Thickness. *J. Mater. Chem. A* **2013**, *1*, 12345−12354.
(19) Etxebarria, I.; Guerrero, A.; Albero, J.; Garcia-Belmonte, G.; Palomares, E.; Pacios, R. Inverted vs Standard PTB7:PC70BM Organic Photovoltaic Devices. The Benefit of Highly Selective and Extracting Contacts in Device Performance. *Org. Electron.* **2014**, *15*, 2756−2762.
(20) Guerrero, A.; Pfannmöller, M.; Kovalenko, A.; Ripolles, T. S.; Heidari, H.; Bals, S.; Kaufmann, L.-D.; Bisquert, J.; Garcia-Belmonte, G. Nanoscale Mapping by Electron Energy-Loss Spectroscopy Reveals Evolution of Organic Solar Cell Contact Selectivity. *Org. Electron.* **2015**, *16*, 227−233.
(21) Tremolet de Villers, B.; Tassone, C. J.; Tolbert, S. H.; Schwartz, B. J. Improving the Reproducibility of P3HT:PCBM Solar Cells by Controlling the PCBM/Cathode Interface. *J. Phys. Chem. C* **2009**, *113*, 18978−18982.
(22) De Sio, A.; Madena, T.; Huber, R.; Parisi, J.; Neyshtadt, S.; Deschler, F.; Da Como, E.; Esposito, S.; von Hauff, E. Solvent Additives for Tuning the Photovoltaic Properties of Polymer−Fullerene Solar Cells. *Sol. Energy Mater. Sol. Cells* **2011**, *95*, 3536−3542.
(23) Lee, S. S.; Loo, Y.-L. Structural Complexities in the Active Layers of Organic Electronics. *Annu. Rev. Chem. Biomol. Eng.* **2010**, *1*, 59−78.
(24) Tress, W.; Leo, K.; Riede, M. Photoconductivity as Loss Mechanism in Organic Solar Cells. *Phys. Status Solidi RRL* **2013**, *7*, 401−405.

DOI: 10.1021/am5071859
ACS Appl. Mater. Interfaces 2015, 7, 1234−1239